Materials Horizons

ROYAL SOCIETY OF CHEMISTRY

COMMUNICATION

View Article Online
View Journal | View Issue

Check for updates

Cite this: *Mater. Horiz.*, 2023, **10**, 3034

Received 14th March 2023,
Accepted 9th May 2023

DOI: 10.1039/d3mh00378g

rsc.li/materials-horizons

Switching magnetic strip orientation using electric fields†

Aitian Chen, [a] Hong-Guang Piao, *[b] Chenhui Zhang,[a] Xiao-Ping Ma,[b] Hanin Algaidi,[a] Yinchang Ma, [a] Yan Li,[a] Dongxing Zheng,[a] Ziqiang Qiu[c] and Xi-Xiang Zhang *[a]

In spintronics, ordered magnetic domains are important for magnetic microdevices and controlling the orientation of ordered magnetic domains is important for applications such as domain wall resistance and spin wave propagation. Although a magnetic field or a current can reorient ordered magnetic domains, an energy-efficient electric-field-driven rotation of the ordered magnetic domains remains elusive. Here, using a nanotrenched polymeric layer, we obtain ordered magnetic strip domains in Ni films on a ferroelectric substrate. By applying electric fields to the ferroelectric substrate, we demonstrate that the ordered magnetic strip domains in Ni films are switched between the *y*- and *x*-axes driven by electric-fields. This switching of magnetic strip orientation is attributed to the electric-field-modulated in-plane magnetic anisotropies along the *x*- and *y*-axes of the Ni films, which are caused by the anisotropic biaxial strain of the ferroelectric substrate *via* strain-mediated magnetoelectric coupling. These results provide an energy-efficient approach for manipulating the ordered magnetic domains using electric fields.

New concepts

Magnetic strip domains enable stable magnetic configurations in the absence of an external magnetic field, which is highly desirable for applications. Although a magnetic field or electric current can be employed to reorient the magnetic strip domains, electric fields are of interest to meet future low power consumption demands. Using patterning stress generated in a nanotrenched PMMA layer *via* magnetoelastic coupling, ordered magnetic strip domains in a Ni film along the *y*-axis are formed on a $Pb(Mg_{1/3}Nb_{2/3})_{0.7}Ti_{0.3}O_3$ (PMN-PT) ferroelectric substrate. Then we demonstrate electric-field-driven continuous rotation of ordered magnetic strip domains in Ni/PMN-PT multiferroic heterostructures *via* strain-mediated magnetoelectric coupling, which originates from modulation of the in-plane magnetic anisotropies along the *x*- and *y*-axes due to the electric-field-induced anisotropic biaxial strain in the PMN-PT ferroelectric substrate. This electric-field switching of magnetic strip orientation is different from other works on controlling magnetic strip domains, where the effect of electric-field-induced piezostrain eliminated the strip domains rather than manipulating their orientation. Our work provides an energy-efficient pathway to switch magnetic strip orientation by electric fields, which will stimulate future efforts toward the electric-field manipulation of domain wall resistance and spin wave propagation in ordered magnetic strip domains that are closely related to their orientation.

Introduction

Microscopic magnetic domains with spontaneous magnetization that align along different directions bridge the gap between the basic macroscopic magnetic properties and applications of magnetic materials.[1,2] The tailoring of magnetic domains is important for both fundamental research and applications. Of the different types of domains, ordered magnetic strip domains[3,4] are interesting with alternating up and down magnetization components, which usually form in magnetic films, such as Ni[5,6] and Permalloy,[3,4] above a critical thickness with a weak out-of-plane magnetic anisotropy. Such magnetic strip domains enable stable magnetic configuration in the absence of an external magnetic field, which is highly desirable for applications. For example, alternating up and down magnetizations in the magnetic strip domains offer an ideal platform to investigate antiferromagnetic-type spin-wave propagation.[7] Moreover, periodic stripe domains having abundant domain walls provide a chance to study domain-wall-based magnetic memory.[8–10] One important feature of magnetic strip domains is their orientations that are closely related to domain wall resistance[8–10] and spin wave propagation[7] such that being able to modulate magnetic strip orientation is important. Although magnetic fields can be employed to reorient the magnetic strip domains,[9,11–13] electrical approaches are of interest to meet future low power consumption demands. Electric currents have

[a] *Physical Science and Engineering Division, King Abdullah University of Science and Technology, Thuwal 23955-6900, Saudi Arabia. E-mail: xixiang.zhang@kaust.edu.sa*
[b] *Department of Physics, College of Science, Yanbian University, Yanji 133002, China. E-mail: hgpiao@ybu.edu.cn*
[c] *Department of Physics, University of California at Berkeley, Berkeley, CA 94720, USA*

† Electronic supplementary information (ESI) available. See DOI: https://doi.org/10.1039/d3mh00378g

recently been injected to control strip domains *via* spin-transfer torque;[8,14,15] however, the manner in which the strip domains can be reoriented only by applying an electric field remains elusive.

Electric fields are considered to be an energy-efficient solution to controlling magnetism.[16–18] In the past decade, considerable progress in the electric-field control of magnetism has been made in multiferroics,[19–21] particularly in ferroelectric/ferromagnetic multiferroic heterostructures with significant magnetoelectric effect at room temperature.[18,22–26] Because of the success of electric-field-controlled in-plane magnetization, researchers have recently attempted to modulate out-of-plane magnetization using electric fields in multiferroic heterostructures *via* strain-mediated magnetoelectric coupling.[27–32] Moreover, studies on multiferroic heterostructures are changing from initially macroscopic magnetic properties,[33,34] *e.g.*, magnetic hysteresis (M–H) loops, to microscopic magnetic domains[35,36] to fulfill future demands for magnetic memory with high density and low power. Magnetic strip domains with alternating up and down magnetization components, which originate from competition between the out-of-plane and in-plane magnetic anisotropies,[30,37] provide a platform to examine microscopic out-of-plane magnetization. Some work[6,30,37–39] has been performed to control magnetic strip domains based on strain-mediated magnetoelectric coupling; however, the effect of electric-field-induced piezostrain eliminated the strip domains[6,30,37] rather than manipulating their orientation. Currently, the electric-field rotation of ordered magnetic strip domains is still not possible.

Herein, we demonstrate the electric-field-driven continuous rotation of ordered magnetic strip domains in Ni/Pb($Mg_{1/3}Nb_{2/3}$)$_{0.7}Ti_{0.3}O_3$ (PMN-PT) multiferroic heterostructures *via* strain-mediated magnetoelectric coupling. Using the patterning stress generated in nanotrenched polymeric layers,[5] we obtained ordered magnetic strip domains in a Ni film on the PMN-PT ferroelectric substrate. While applying electric fields to the PMN-PT substrate, the orientation of the ordered magnetic strip domains continuously rotated from the *y*-axis to the *x*-axis as observed *via* magnetic force microscopy (MFM). Micromagnetic simulations demonstrated that these continuous electric-field-rotated ordered magnetic strip domains were caused by the electric-field-induced continuous modulation of the in-plane magnetic anisotropies along the *x*- and *y*-axes because of the anisotropic biaxial strain of the PMN-PT ferroelectric substrate. Moreover, we observed electric-field-induced annihilation of magnetic strip domains in Ni films because of the enhancement of the in-plane magnetic anisotropy. These results indicate the important role of in-plane magnetic anisotropy for ordered magnetic strip domains and offer an energy-efficient approach to tailoring ordered magnetic strip domains *via* magnetoelectric coupling.

Results and discussion

Formation and modulation of ordered magnetic strip domains in Ni/PMN-PT multiferroic heterostructures

In general, the orientations of the spontaneous magnetic strip domains are random such that external stimuli are required to align them to form ordered magnetic strip domains. Recently, Zhang *et al.*[5] reported a method using the patterning stress in nanotrenched polymeric layers to form ordered magnetic strip domains. Using a similar method, we fabricated Ni/PMN-PT multiferroic heterostructures having ordered magnetic strip domains, as illustrated in Fig. 1a. Ti/Au layers were first deposited on the top and bottom of (011)-oriented PMN-PT ferroelectric substrates as electrodes for applying electric fields to generate strain. Then, nanotrenches having a width of 200 nm were patterned into a 200 nm-thick poly(methyl methacrylate) (PMMA) layer on the PMN-PT using electron beam lithography. Finally, a 120 nm-thick Ni magnetic film was evaporated to form ordered magnetic strip domains. It should be noted that the 200 nm-thick PMMA layer does not affect the transfer of piezostrain into the Ni magnetic layer since the strain is a long-range order parameter[23] and can transfer more than 10 μm.[40] Fig. 1b shows an atomic force microscopy (AFM) image with a nanotrench along the *x*-direction of the PMN-PT substrate. As shown in Fig. 1a, the *x*-, *y*-, and *z*-axes denote the pseudocubic [100], [01$\bar{1}$], and [011] crystallographic directions of the PMN-PT substrate, respectively. Fig. 1c shows the corresponding magnetic domain structure without an electric field (0 kV cm^{-1}). The ordered magnetic strip domains whose orientation is perpendicular to the nanotrench, *i.e.*, along the *y*-direction, formed surrounding the nanotrench. It is well known that magnetic strip domains originate from the competition between a moderate out-of-plane magnetic anisotropy and the in-plane shape anisotropy.[11,30] The out-of-plane magnetic anisotropy is understood to result from an isotropic planar growth stress.[1,30,37] The competition between the out-of-plane and in-plane magnetic anisotropies results in alternating up and down magnetization components, as illustrated in Fig. 1a, to form magnetic strip domains and to give a strong contrast in MFM images. Note that the magnetic strip domains near the nanotrench were blurry; this may be caused by the large local stress near the nanotrench. These ordered strip domains, generated given the assistance of a PMMA nanotrench, agree with previous results.[5]

To examine the effect of an electric field on the ordered magnetic strip domains, we performed *in situ* MFM measurements with electric fields. Fig. 1d shows the MFM image with an applied electric field of 15 kV cm^{-1}. Note that the orientation of the ordered strip domains was nearly along the *x*-axis. Comparing the MFM images in Fig. 1c and d, two important differences in the domain structure are reported because of the application of an electric field. (i) The reorientation of the ordered magnetic strip domains from the *y*-axis to *x*-axis, which can be clearly seen in the area highlighted by the red dashed-line box. (ii) The annihilation of the magnetic strip domains and the appearance of dark lines in the area highlighted by the blue dashed-line box. These two changes are closely related to the electric-field modulation of the magnetic anisotropy in the Ni film.

Because the orientation of the ordered magnetic strip domains is closely related to the in-plane magnetic anisotropy,[5] local in-plane M–H loops of the Ni film in the region near the nanotrench were obtained using the magneto-optic Kerr effect, as shown in Fig. 1e.

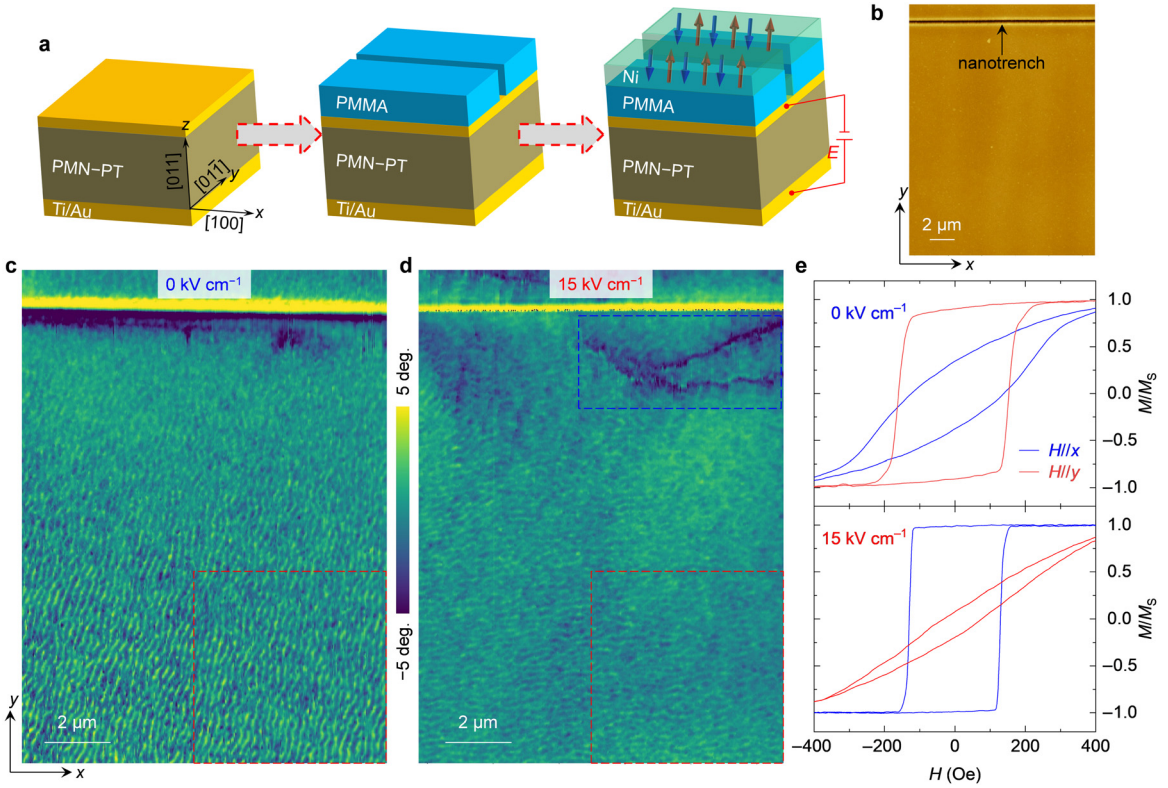

Fig. 1 Modulation of the ordered magnetic strip domains by electric fields *via* strain-mediated magnetoelectric coupling. (a) Formation of the ordered magnetic strip domains in the Ni films on the PMN-PT substrate using a PMMA nanotrench. The arrows illustrate the alternating up (red) and down (blue) magnetization components in the strip domains. The *x*-, *y*-, and *z*-axes denote the pseudocubic [100], [01$\bar{1}$], and [011] crystallographic directions of PMN-PT, respectively. The electric fields were applied to the PMN-PT ferroelectric substrate to generate piezostrain to tailor the ordered magnetic strip domains in the Ni film by modulating its magnetic anisotropy. (b) AFM image of a PMMA nanotrench along the *x*-axis on the PMN-PT substrate. (c and d) Magnetic domain images of the Ni film at 0 kV cm^{-1} (c) and 15 kV cm^{-1} (d). Because of the alternating up and down magnetization components, the magnetic strip domains have a strong contrast in the MFM images. The red dashed-line box highlights the area of the electric-field-rotated magnetic strip domains and the blue dashed-line box shows the annihilation of the magnetic strip domains. (e) M–H loops measured with the magnetic field applied along the *x*- and *y*-axes at 0 kV cm^{-1} and 15 kV cm^{-1}, suggesting a distinct rotation of the magnetic easy axis driven by the electric field.

At 0 kV cm^{-1}, the M–H loop was square and smooth as measured by applying a magnetic field along the *y*-axis but was gradual along the *x*-axis. This indicates a uniaxial in-plane magnetic anisotropy with the magnetic easy axis along the *y*-direction. The large remnant magnetization of the M–H loop measured along the *y*-axis suggests that there are in-plane magnetization components lying along the *y*-axis despite the alternating out-of-plane magnetization components.[38,41] This in-plane magnetic anisotropy K_{y0} is attributed to the local stress generated by the PMMA nanotrench *via* magnetoelastic coupling.[5] The K_{y0} value was $\sim 11 \times 10^3$ J m^{-3} as can be determined from the M–H loops along the *y*- and *x*-axes at 0 kV cm^{-1} in Fig. 1e using the area method.[42] At 15 kV cm^{-1}, however, the M–H loop was square along the *x*-axis but gradual and smooth along the *y*-axis. This sharp contrast in the M–H loops indicates the rotation of the magnetic easy axis driven by the electric fields and should lead to the two aforementioned distinct changes in the ordered magnetic strip domains in Fig. 1c and d.

Electric-field-driven continuous rotation of ordered magnetic strip domains

We first focus on the electric-field-driven reorientation of the ordered magnetic strip domains. Fig. 2a shows the evolution of the ordered magnetic strip domains (the red regions in Fig. 1c and d) under various electric fields. Note that the ferroelectric domains do not switch solely by applying positive electric fields. Apparently, the orientation of the ordered strip domains continuously rotated from the *y*-axis to the *x*-axis when increasing the applied electric fields and switched back to the *y*-axis after removing the applied electric field (Fig. S1, ESI†). Such a rotation can be clearly seen from a two-dimensional fast Fourier transform analysis of the MFM image, as shown in Fig. 2b. The electric-field dependent average angle of the strip domains exhibited a continuous rotation driven by the electric field (Fig. 2c), where the *x*-direction is defined as 0°. Conventionally, a magnetic field[9,11–13] is used to reorient the strip domains or an electric current with spin-transfer torque is injected to control the orientation of the magnetic strip domains.[8,14,15] Although strain-mediated magnetoelectric coupling has been used to manipulate magnetic strip domains,[6,30,37–39] an electric field usually destroys the strip domains rather than manipulating their orientation.[6,30,37] To the best of our knowledge, the continuous rotation of strip domains driven by electric fields has not yet been reported. Additionally, modulating strip domains using an electric field is more energy efficient than that by

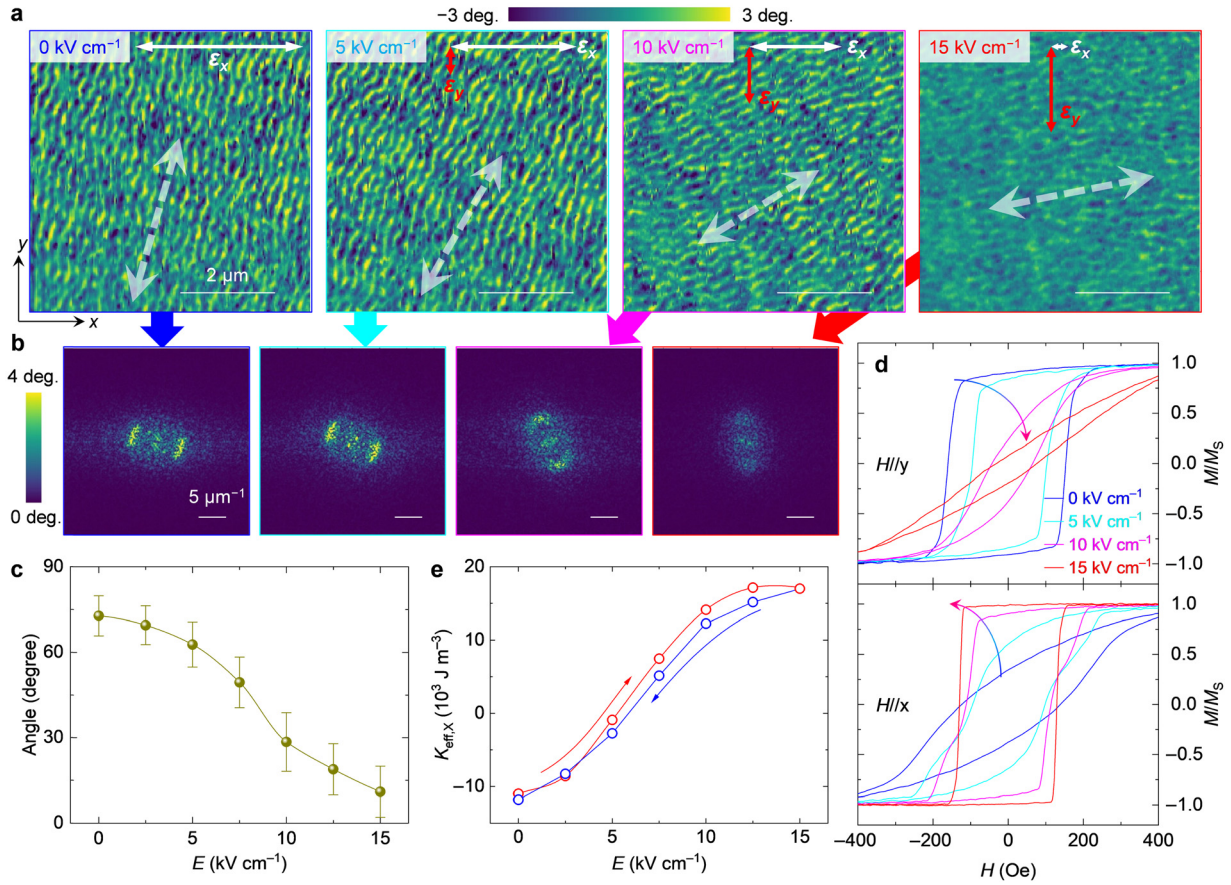

Fig. 2 Continuous rotation of the ordered magnetic strip domains driven by electric fields. (a) Evolution of the ordered magnetic strip domains with increasing electric fields. The white dashed double-headed arrows show the orientations of the ordered magnetic strip domains. The solid double-headed arrows illustrate the directions of the tensile strain along the *x* (white) and *y* (red) axes. At 0 kV cm^{-1}, a large tensile strain originates from the PMMA nanotrench.[5] Applying an electric field generates a compressive strain along the *x*-axis and a tensile strain along the *y*-axis. So the tensile strain decreases along the *x*-axis and increases along the *y*-axis when increasing the electric fields. (b) Two-dimensional fast Fourier transform analysis of the MFM images in panel (a). (c) Dependence of the average angle of the ordered strip domains on the applied electric field, which indicates a continuous rotation, with 0° defined along the *x*-direction. (d) *In situ* M–H loops measured along the *x*- and *y*-axes at various electric fields, suggesting a gradual change in the magnetic easy axis from the *y*-axis to the *x*-axis. The arrows show the trend of the M–H loops with increasing electric fields. (e) Electric-field dependence of the effective in-plane magnetic anisotropy along the *x*-axis, which exhibits a linear and reversible behavior. The arrows indicate the sweeping directions of the electric fields.

spin-transfer torque (Note S1, ESI†). This indicates that our work is extremely significant compared with previous studies that have achieved slight modulations of the strip domains *via* magnetoelectric coupling.[6,30,37–39] In previous studies,[6,30,37–39] the magnetic films were directly deposited on the ferroelectric substrate; however, we inserted a 200 nm-thick PMMA layer between the PMN-PT and the Ni film in this work. It has been reported that inserting a 10 μm polymer between the PMN-PT substrate and Ni magnetic film can enhance magnetoelectric coupling in comparison with that without a polymer.[40] We directly deposited a 120 nm-thick Ni film on the PMN-PT and found that the orientation of the magnetic strip was not affected noticeably by the applied electric fields (Fig. S2, ESI†), which is consistent with the previous studies.[6,30,37–39] So the rotation of magnetic strips by electric fields (Fig. 2a) is closely related to the inserted PMMA layer between the PMN-PT substrate and Ni film. Moreover, note that the local uniform strain generated by the nanotrenched PMMA aligns the magnetic strip making it easily and coherently rotate under external piezostrain. This could be the reason that the electric-field-induced strain can successfully manipulate the orientation of the strip domains in our work using nanotrenched PMMA, which makes our results different from that in the previous studies without nanotrenched PMMA.[6,30,37–39]

Because the orientation of the ordered magnetic strip domains is closely related to the in-plane magnetic anisotropy,[5] we measured *in situ* in-plane M–H loops with various electric fields, as shown in Fig. 2d. When measured with a magnetic field along the *y*-axis, the M–H loop was square with a sharp magnetization switching at 0 kV cm^{-1}. The increase in the electric field strength reduced the coercive field (H_C) and the remnant magnetization; the loop was then gradual and smooth at 15 kV cm^{-1}. However, when measured with a magnetic field along the *x*-axis, the M–H loop was gradual and smooth at 0 kV cm^{-1} and increasing electric field strength made the loops squarer with an increase in remnant magnetization. These results indicate that the increase in the electric field strength gradually rotated the magnetic easy axis

from the *y*-axis to the *x*-axis. We then extracted the effective in-plane magnetic anisotropy ($K_{\mathrm{eff},x}$) from the M–H loops along the *y*- and *x*-axes using the area method[42] at each electric field, as shown in Fig. 2e. The dependence of $K_{\mathrm{eff},x}$ on the electric field was reversible and nearly linear despite a small hysteresis, which is attributed to the electric-field-induced magnetoelastic anisotropy *via* strain-mediated magnetoelectric coupling. The magnetoelastic anisotropy can be expressed as follows:[43,44]

$$K = \frac{3}{2}\lambda Y \varepsilon, \tag{1}$$

where λ and Y are the magnetostriction coefficient and the Young's modulus of the Ni film, respectively, and ε is the strain. For (011)-oriented PMN-PT substrates, the electric-field-induced piezostrain along the *x*- and *y*-axes can be written as follows:[30]

$$\begin{aligned} \varepsilon_x &= d_{31} \times E \\ \varepsilon_y &= d_{32} \times E \end{aligned} \tag{2}$$

where the piezoelectric coefficients[45] are $d_{31} = -1883$ pC N^{-1} and $d_{32} = 610$ pC N^{-1} and E is the applied electric field. Therefore, applying an electric field induces a linear anisotropic biaxial strain, *i.e.*, a compressive strain along the *x*-axis and a simultaneous tensile strain along the *y*-axis,[46,47] as shown in Fig. 3a; the effective compressive strain $\varepsilon_x - \varepsilon_y$ increases as the electric field increases. Because increasing the electric field enhances the effective compressive strain along the *x*-axis, it is reasonable that $K_{\mathrm{eff},x}$ increases with increasing electric field, as shown in Fig. 2e, considering that λ in the Ni film is negative.[30,37]

To gain further insight in the electric-field rotation of the ordered strip domains in Fig. 2a, we calculated the distribution of the normalized magnetization (m) in Ni films under various electric fields *via* the Landau–Lifshitz–Gilbert equation:[5,43,48]

$$\frac{\mathrm{d}\mathbf{m}}{\mathrm{d}t} = -\gamma \mathbf{m} \times \mathbf{H}_{\mathrm{eff}} + \alpha \mathbf{m} \times \frac{\mathrm{d}\mathbf{m}}{\mathrm{d}t}, \tag{3}$$

where γ is the gyromagnetic ratio and α is the Gilbert damping constant. Note that $\mathbf{H}_{\mathrm{eff}}$ is the effective magnetic field, where $\mathbf{H}_{\mathrm{eff}} = \frac{\partial E_{\mathrm{tot}}}{\partial \mathbf{m}}$. Here, E_{tot} is the total magnetic energy of the system including the Zeeman, exchange, demagnetization, and magnetoelastic energies.[49] The in-plane magnetoelastic energy comprises *x*- and *y*-components: K_x and K_y. The Ni film is mainly affected by the initial strain from the PMMA nano-trench and the electric-field-induced piezostrain, so the magnetic anisotropy of the Ni film under an electric field can be considered the sum of the initial K_{y0} and the electric-field-induced magnetoelastic anisotropy. For simplicity, we assume that the effect of electric field on K_{y0} is negligibly small. Thus, K_x and K_y at each electric field can be expressed as follows:

$$\begin{aligned} K_x &= \frac{3}{2}\lambda Y \varepsilon_x \\ K_y &= K_{y0} + \frac{3}{2}\lambda Y \varepsilon_y, \end{aligned} \tag{4}$$

where ε_x and ε_y are the electric-field-induced piezostrains along the *x*- and *y*-axes, respectively, in the (011)-oriented PMN-PT substrate as expressed by eqn (2). Therefore, we can obtain the

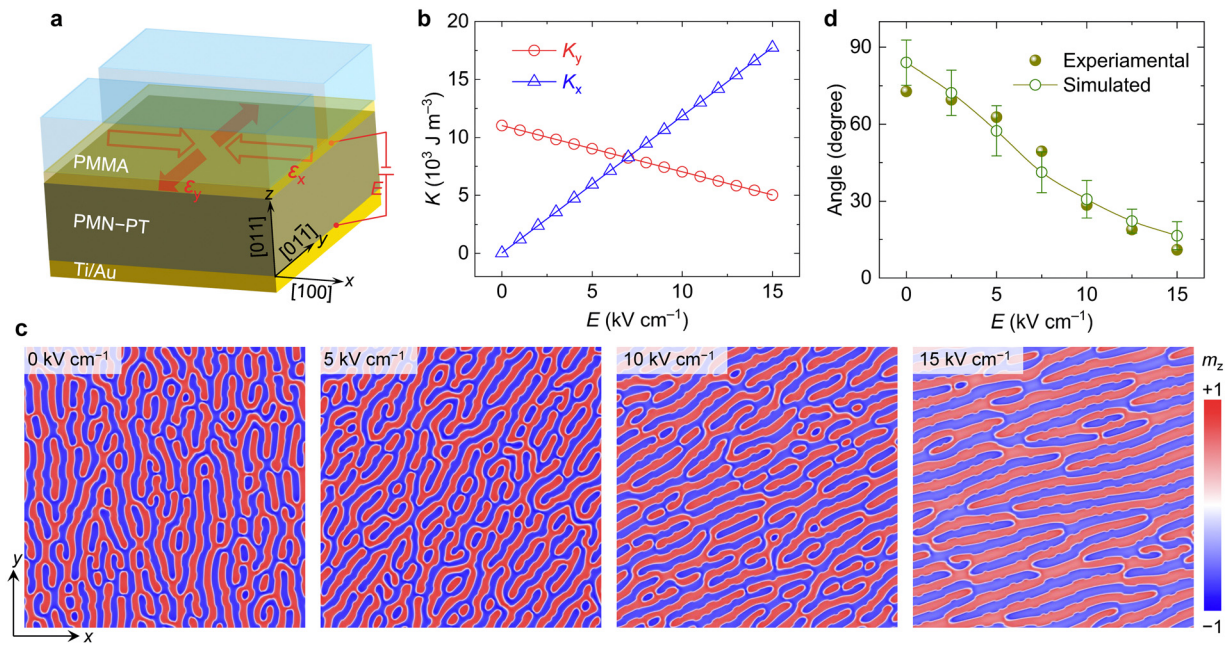

Fig. 3 Simulated electric-field-driven rotation of the ordered strip magnetic domains *via* the modulation of the in-plane magnetic anisotropies. (a) Illustration of the electric-field-induced anisotropic biaxial strain in the PMN-PT ferroelectric substrate *via* the converse piezoelectric effect, *i.e.*, a compressive strain ε_x along the *x*-axis and a simultaneous tensile strain ε_y along the *y*-axis. (b) Dependence of K_x and K_y on the electric field strength obtained from eqn (2) and (4). (c) Simulated m_z of the normalized magnetization under various electric fields using K_x and K_y from panel (b). It is evident that applying electric fields continuously rotated the orientation of the ordered magnetic strip domains from the *y*-axis to the *x*-axis *via* the modulation of K_x and K_y. (d) Simulated and experimental average angles of the ordered strip domains as a function of the electric field, showing good consistency.

electric-field-dependent K_x and K_y (Fig. 3b) using eqn (2) and (4) with the Ni film's magnetostriction coefficient[30,37] $\lambda = -32.9 \times 10^{-6}$ and Young's modulus $Y = 133$ GPa. Using the K_x and K_y values in Fig. 3b, we visualized the distribution of the magnetic strip domains in the Ni films under different electric fields with the out-of-plane magnetization component (m_z), as shown in Fig. 3c. Without an electric field, the ordered strip domains are roughly oriented along the *y*-axis because of the action of K_{y0}. It has been shown that the ratio of K_x/K_y is closely related to the orientation of the strip domains and the effective in-plane magnetic anisotropy K_{in} is the vectorial sum of K_x and K_y.[5] The application of an electric field changes the ratio of K_x/K_y by decreasing K_y and increasing K_x (Fig. 3b), which modulates the easy axis of K_{in},[50] such that the orientation of the strip domains is rotated away from the *y*-axis as the electric field increases and is nearly along the *x*-axis at 15 kV cm^{-1}. The electric-field-dependent average angle of the ordered strip domains was obtained from the simulation results (Fig. 3c) and is plotted in Fig. 3d. This result agrees well with the experimental average angle extracted from the MFM images in Fig. 2a. These simulations indicate that the electric-field-driven continuous rotation of the ordered strip domains in the Ni films are caused by the modulation of the in-plane magnetic anisotropies along the *y*- and *x*-axes, which was induced by the anisotropic biaxial piezostrain of the PMN-PT ferroelectric substrate *via* strain-mediated magnetoelectric coupling.

Electric-field-induced annihilation of magnetic strip domains

We believe that the annihilation of the magnetic strip domains highlighted in the blue dashed-line box in Fig. 1d originates from the electric-field-induced enhancement of the in-plane magnetic anisotropy. To confirm this speculation, we changed the PMMA nanotrench from along the *x*-axis to along the *y*-axis, as shown in Fig. 4a. In this configuration, the magnetoelastic anisotropies both induced by the electric fields and generated by the PMMA nanotrench were along the *x*-axis such that they could add together to enhance the in-plane magnetic anisotropy along the *x*-axis. Fig. 4b shows a PMMA nanotrench along the *y*-direction of the PMN-PT substrate. Fig. 4c shows the corresponding MFM images under different electric fields. Note that certain dark lines appeared near the nanotrench at 0 kV cm^{-1} and gradually grew at 5 kV cm^{-1}. When the electric field was >10 kV cm^{-1}, the dark line in the blue dashed-box propagated to the region away from the nanotrench. Moreover, note that, in the red dashed box, the dark lines appeared until 10 kV cm^{-1} and then dramatically spread when the electric field strength was increased to 15 kV cm^{-1}. The dark lines could disappear after removing the applied electric field (Fig. S3, ESI†). It should be pointed out that such changes in the MFM images are not from surface morphology, because the morphology was not affected by the applied electric fields (Fig. S4, ESI†). The magnetic strip domains with alternating up and down magnetization components can be clearly imaged *via* MFM, which is sensitive to the out-of-plane magnetization.[51] For the area near the dark lines, the magnetic strip domains disappear and the domain structure cannot be identified *via* MFM, indicating the absence of an out-of-plane magnetization. These results suggest that increasing the electric field strength eliminates the magnetic strip domains. Moreover, the dark lines in Fig. 4c and 1d always appeared along the *x*-axis, which is the orientation of the magnetic easy axis, indicating its close correlation with the in-plane magnetic anisotropy.

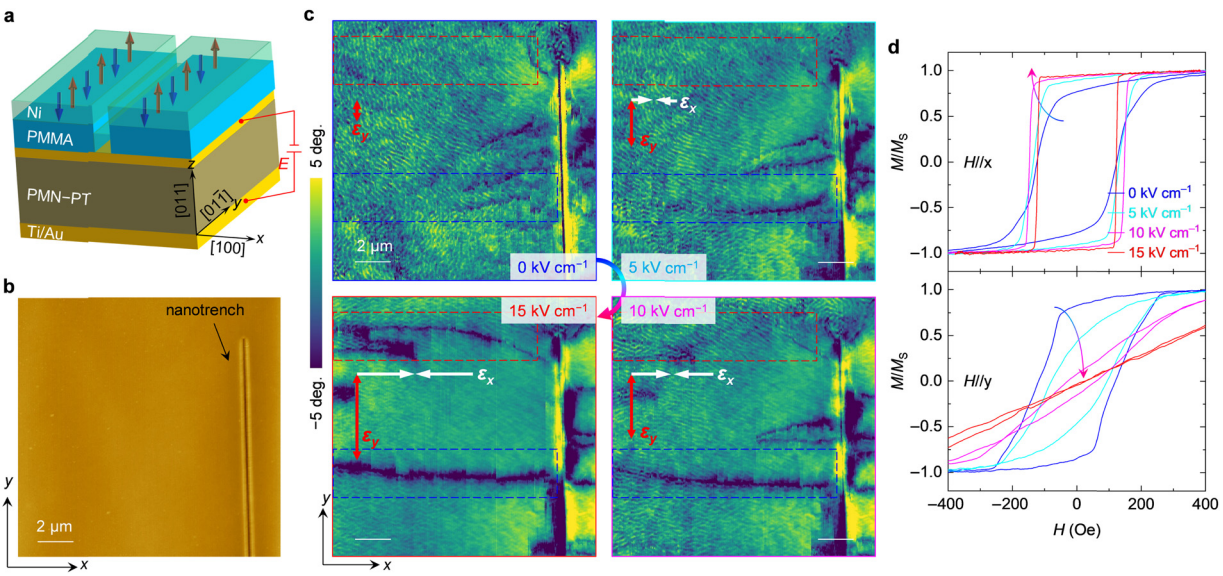

Fig. 4 Electric-field-induced annihilation of the magnetic strip domains. (a and b) Schematic (a) and AFM image (b) of Ni film deposited on the PMN-PT substrate with a PMMA nanotrench along the *y*-axis. The arrows in (a) illustrate the alternating up (red) and down (blue) magnetization components in the strip domains. (c) Magnetic domain images of the Ni film with increasing electric fields. The dashed-line boxes show how the magnetic strip domains were annihilated when increasing the applied electric fields. The solid arrows illustrate the directions of the compressive strain along the *x*-axis (white) and the tensile strain along the *y*-axis (red). (d) *In situ* M–H loops measured along the *x*- and *y*-axes under various electric fields. The arrows show the trend of the M–H loops with increasing electric fields.

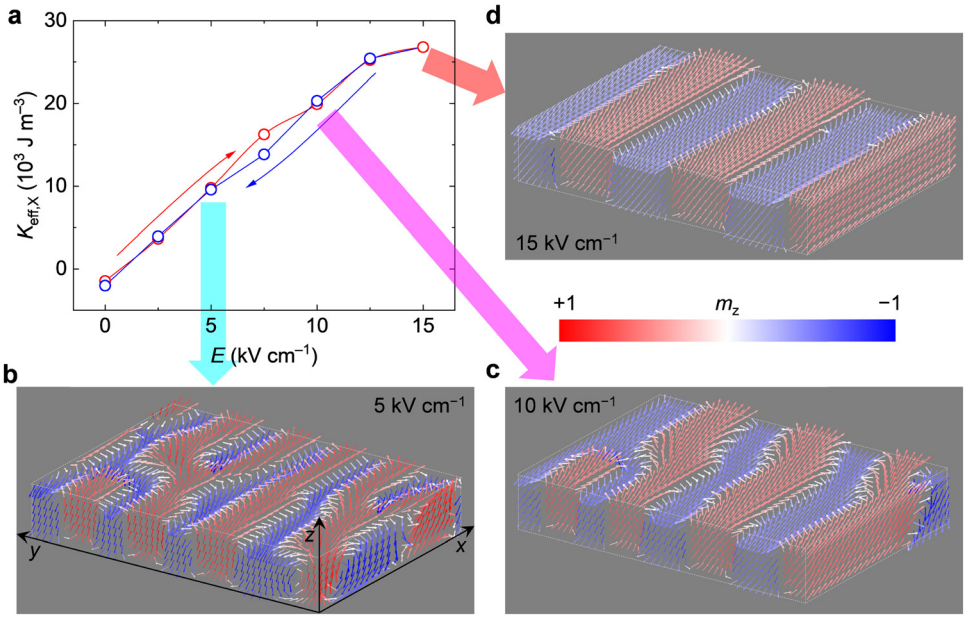

Fig. 5 Suppression of the out-of-plane magnetization component as a result of the enhancement of the in-plane magnetic anisotropy. (a) Electric-field-dependence of the effective in-plane magnetic anisotropy along the *x*-axis deduced from Fig. 4d, which displays linear and reversible behavior. The arrows indicate the sweeping directions of the electric fields. (b–d) Simulated domain structures at various electric fields. It can be seen that the out-of-plane magnetization component decreased as the applied electric field increased because of the enhanced in-plane magnetic anisotropy. At 15 kV cm^{-1} with an in-plane magnetic anisotropy larger than 20×10^3 J m^{-3}, the out-of-plane magnetization components significantly decreased resulting in the annihilation of the magnetic strip domains, as revealed by MFM.

We measured *in situ* M–H loops with electric fields to examine the in-plane magnetic anisotropy of the Ni films on the nanotrenched PMMA along the *y*-direction. As shown in Fig. 4d, the profiles of the M–H loops measured along the *x*-axis were square and magnetization switching became increasingly sharp at larger electric fields. However, the M–H loops measured along the *y*-axis became increasingly gradual at larger electric fields with a decreasing remanent magnetization and an increasing saturation magnetic field. These results suggest that the electric field enhanced the in-plane magnetic anisotropy along the *x*-axis. The electric-field-dependence of $K_{eff,X}$, which was deduced from the M–H loops along the *y*- and *x*-axes in Fig. 5a using the area method, exhibited reversible and linear behavior, as shown in Fig. 5a.

We then performed micromagnetic simulations to investigate the effect of in-plane magnetic anisotropy on the domain structures. At 5 kV cm^{-1} with $K_{eff,X} \sim 10 \times 10^3$ J m^{-3}, the simulation in Fig. 5b shows strip domains with significant out-of-plane magnetization. When increasing the electric field strength to 10 kV cm^{-1} with $K_{eff,X} \sim 20 \times 10^3$ J m^{-3}, the out-of-plane magnetization decreases (Fig. 5c). On additional increase in $K_{eff,X}$ by applying an electric field of 15 kV cm^{-1}, the magnetization points nearly in the *x*-axis, as shown in Fig. 5d. Although there is a tiny out-of-plane magnetization component, it is hard to be detected using MFM. Therefore, the electric-field-enhanced in-plane $K_{eff,X}$ suppresses the out-of-plane magnetization, thus resulting in the annihilation of the magnetic strip domains. Moreover, note that the dark lines dramatically appeared after 10 kV cm^{-1} in Fig. 4c with $K_{eff,X}$ approximately equal to 20×10^3 J m^{-3} (Fig. 4d); however, $K_{eff,X}$ was $<17 \times 10^3$ J m^{-3} for the Ni films on the nanotrenched PMMA along the *x*-axis (Fig. 2e). Therefore, it is reasonable that we primarily observed the electric-field-rotated ordered strip domains of the Ni films on the nanotrenched PMMA along the *x*-direction, as shown in Fig. 2a.

Conclusions

We demonstrate the electric-field-driven continuous rotation of ordered magnetic strip domains in Ni/PMN-PT multiferroic heterostructures *via* strain-mediated magnetoelectric coupling. The ordered magnetic strip domains in the Ni film along the *y*-axis were formed on the PMN-PT substrate using patterning stress generated in a nanotrenched PMMA layer *via* magnetoelastic coupling. By applying electric fields to the PMN-PT ferroelectric substrate to generate anisotropic biaxial piezostrain, we observed continuous rotation of the ordered magnetic strip domains from the *y*-axis to the *x*-axis as identified by MFM. Micromagnetic simulations demonstrated that these continuous electric-field-rotated ordered magnetic strip domains originated from the electric-field-induced anisotropic biaxial strain in the PMN-PT ferroelectric substrate, which modulated the in-plane magnetic anisotropies along the *x*- and *y*-axes *via* strain-mediated magnetoelectric coupling. These results provide an energy-efficient pathway to realize the electric-field reorientation of ordered magnetic strip domains by tuning the in-plane magnetic anisotropies. Note that previous work mainly focused

on electric-field control of local magnetizations[52–54] while we investigated electric-field-modulated orientation of ordered magnetic strip domains. Since orientation of ordered magnetic strip domains is important for domain wall resistance[8–10] and spin wave propagation,[7] we expect that our results will stimulate future efforts toward the electric-field manipulation of domain wall resistance and spin wave propagation in ordered magnetic strip domains.

Experimental section

Sample fabrication

The samples were deposited on (011)-oriented PMN-PT single crystals with a typical size of 5 mm × 6 mm × 0.2 mm (Hefei Kejing Materials Technology Co., Ltd, China). To apply electric fields on the PMN-PT substrate to realize strain-mediated magnetoelectric coupling, Ti (3 nm) and Au (10 nm) were first deposited *via* magnetron sputtering on the top of the PMN-PT substrates as the top electrode, and Ti (10 nm) and Au (150 nm) were sputtered on the bottom of the PMN-PT substrate as the bottom electrode. A 200 nm-thick layer of PMMA (MircoChem, 495 PMMA A4) was spin-coated on the PMN-PT substrate (2000 rpm for 60 s) and prebaked at 180 °C on a hot plate for 60 s. Nanotrenches were patterned using electron beam lithography (EBL, Crestec CABL-9000) and then developed in a solution of methyl isobutyl ketone/isopropanol for 60 s, rinsed with isopropanol, and dried in a nitrogen stream. Subsequently, a 120 nm-thick Ni film, as determined using a quartz microbalance, was deposited *via* electron beam evaporation (Denton Vacuum Explorer) and was then capped with a 10 nm-thick layer of Ti to prevent oxidation.

Magnetic characteristics

MFM experiments were performed on an Agilent 5500 system under ambient conditions using a PPP-MFMR probe (Nanosensors) with a lift height of 50 nm. Owing to the PMMA nanotrench, the spontaneous ordered strip domains can be obtained without the help of a magnetic field.[5] So the MFM measurements were performed at zero magnetic field immediately after the deposition of the Ni films without applying a magnetic field. All MFM data analyses were performed using Gwyddion 2.60.[55] The M–H loops were collected using a Durham Nano-MOKE 2. All of the measurements were performed at room temperature with *in situ* electric fields using a Keithley 6517 electrometer.

Micromagnetic simulations

Simulations using MuMax3[48] were performed to explore the change in the magnetic domain configurations of the Ni film under the electric-field-induced strain. For all simulations, a 5.0 μm × 5.0 μm × 0.12 μm film structure was considered with the unit cell dimension set to 5 nm × 5 nm × 5 nm. The parameters of the Ni film were as follows:[5] the exchange stiffness coefficient was $A = 13 \times 10^{-12}$ J m^{-1}, the saturation magnetization was $M_S = 8.6 \times 10^5$ A m^{-1}, the Gilbert damping constant was $\alpha = 0.1$, and the out-of-plane magnetic anisotropy constant without an electric field was set to $K_U = 1.0 \times 10^5$ J m^{-3}. Because the out-of-plane magnetic anisotropy of the Ni films weakens with increasing electric field strength,[37] we defined the uniaxial anisotropy K_U in the Ni film as being composed of *x*-, *y*-, and *z*-components, *i.e.*, $K_U = \sqrt{K_x^2 + K_y^2 + K_z^2}$.

Author contributions

A. C. conceived the idea, designed the experiments and X.-X. Z. supervised the project. A. C. deposited the Ni film, and performed the MFM and MOKE measurements. C. Z. and H. A performed the electron beam lithography. H.-G. P. and X.-P. M. performed the micromagnetic simulations. A. C. and X.-X. Z. analyzed the data and wrote the manuscript. All the authors read and commented on the manuscript.

Conflicts of interest

The authors declare no conflicts of interest.

Acknowledgements

This work was supported by King Abdullah University of Science and Technology (KAUST) Office of Sponsored Research (OSR) under Award No. ORA-CRG8-2019-4081 and ORA-CRG10-2021-4665. The authors acknowledge the Core Lab at KAUST for their excellent assistance.

References

1 A. Hubert and R. Schäfer, *Magnetic domains: the analysis of magnetic microstructures*, Springer-Verlag, Berlin, 1998.
2 R. C. O'Handley, *Modern magnetic materials: principles and applications*, John Wiley & Sons, New York, 2000.
3 R. J. Spain, *Appl. Phys. Lett.*, 1965, **6**, 8–9.
4 N. Saito, H. Fujiwara and Y. Sugita, *J. Phys. Soc. Jpn.*, 1964, **19**, 1116–1125.
5 J. Zhang, W. K. Lee, R. Tu, D. Rhee, R. Zhao, X. Wang, X. Liu, X. Hu, X. Zhang, T. W. Odom and M. Yan, *Nano Lett.*, 2021, **21**, 5430–5437.
6 J. L. Hockel and G. P. Carman, *Appl. Phys. Lett.*, 2012, **100**, 092902.
7 C. Liu, S. Wu, J. Zhang, J. Chen, J. Ding, J. Ma, Y. Zhang, Y. Sun, S. Tu, H. Wang, P. Liu, C. Li, Y. Jiang, P. Gao, D. Yu, J. Xiao, R. Duine, M. Wu, C. W. Nan, J. Zhang and H. Yu, *Nat. Nanotechnol.*, 2019, **14**, 691–697.
8 S. Wu, Y. Zhang, C. Tian, J. Zhang, M. Wu, Y. Wang, P. Gao, H. Yu, Y. Jiang, J. Wang, K. Meng and J. Zhang, *ACS Appl. Mater. Interfaces*, 2021, **13**, 23945–23950.
9 R. Danneau, P. Warin, J. P. Attane, I. Petej, C. Beigne, C. Fermon, O. Klein, A. Marty, F. Ott, Y. Samson and M. Viret, *Phys. Rev. Lett.*, 2002, **88**, 157201.
10 A. D. Kent, J. Yu, U. Rüdiger and S. S. P. Parkin, *J. Phys.: Condens. Matter*, 2001, **13**, R461–R488.

11 S. Fin, R. Tomasello, D. Bisero, M. Marangolo, M. Sacchi, H. Popescu, M. Eddrief, C. Hepburn, G. Finocchio, M. Carpentieri, A. Rettori, M. G. Pini and S. Tacchi, *Phys. Rev. B: Condens. Matter Mater. Phys.*, 2015, **92**, 224411.
12 L.-C. Garnier, M. Marangolo, M. Eddrief, D. Bisero, S. Fin, F. Casoli, M. G. Pini, A. Rettori and S. Tacchi, *J. Phys.: Mater.*, 2020, **3**, 024001.
13 R. Salikhov, F. Samad, B. Böhm, S. Schneider, D. Pohl, B. Rellinghaus, A. Ullrich, M. Albrecht, J. Lindner, N. S. Kiselev and O. Hellwig, *Phys. Rev. Appl.*, 2021, **16**, 034016.
14 J. Wang, S. Wu, J. Ma, L. Xie, C. Wang, I. A. Malik, Y. Zhang, K. Xia, C.-W. Nan and J. Zhang, *Appl. Phys. Lett.*, 2018, **112**, 072408.
15 J. Wang, L. S. Xie, C. S. Wang, H. Z. Zhang, L. Shu, J. Bai, Y. S. Chai, X. Zhao, J. C. Nie, C. B. Cao, C. Z. Gu, C. M. Xiong, Y. Sun, J. Shi, S. Salahuddin, K. Xia, C. W. Nan and J. X. Zhang, *Phys. Rev. B: Condens. Matter Mater. Phys.*, 2014, **90**, 224407.
16 F. Matsukura, Y. Tokura and H. Ohno, *Nat. Nanotechnol.*, 2015, **10**, 209–220.
17 C. Song, B. Cui, F. Li, X. Zhou and F. Pan, *Prog. Mater. Sci.*, 2017, **87**, 33–82.
18 C. A. Vaz, *J. Phys.: Condens. Matter*, 2012, **24**, 333201.
19 N. A. Spaldin and R. Ramesh, *Nat. Mater.*, 2019, **18**, 203–212.
20 M. Fiebig, T. Lottermoser, D. Meier and M. Trassin, *Nat. Rev. Mater.*, 2016, **1**, 16046.
21 S. Dong, J.-M. Liu, S.-W. Cheong and Z. Ren, *Adv. Phys.*, 2015, **64**, 519–626.
22 S. Bandyopadhyay, J. Atulasimha and A. Barman, *Appl. Phys. Rev.*, 2021, **8**, 041323.
23 J. M. Hu, L. Q. Chen and C. W. Nan, *Adv. Mater.*, 2016, **28**, 15–39.
24 T. Taniyama, *J. Phys.: Condens. Matter*, 2015, **27**, 504001.
25 N. X. Sun and G. Srinivasan, *Spin*, 2012, **02**, 1240004.
26 A. T. Chen and Y. G. Zhao, *APL Mater.*, 2016, **4**, 032303.
27 Y. Sun, Y. Ba, A. Chen, W. He, W. Wang, X. Zheng, L. Zou, Y. Zhang, Q. Yang, L. Yan, C. Feng, Q. Zhang, J. Cai, W. Wu, M. Liu, L. Gu, Z. Cheng, C. W. Nan, Z. Qiu, Y. Wu, J. Li and Y. Zhao, *ACS Appl. Mater. Interfaces*, 2017, **9**, 10855–10864.
28 B. Peng, Z. Zhou, T. Nan, G. Dong, M. Feng, Q. Yang, X. Wang, S. Zhao, D. Xian, Z. D. Jiang, W. Ren, Z. G. Ye, N. X. Sun and M. Liu, *ACS Nano*, 2017, **11**, 4337–4345.
29 A. T. Chen, H. L. Huang, Y. Wen, W. Y. Liu, S. F. Zhang, J. Kosel, W. D. Sun, Y. G. Zhao, Y. L. Lu and X. X. Zhang, *Mater. Horiz.*, 2020, **7**, 2328–2335.
30 M. Ghidini, F. Maccherozzi, X. Moya, L. C. Phillips, W. Yan, J. Soussi, N. Metallier, M. E. Vickers, N. J. Steinke, R. Mansell, C. H. Barnes, S. S. Dhesi and N. D. Mathur, *Adv. Mater.*, 2015, **27**, 1460–1465.
31 A. Chen, S. Zhang, Y. Wen, H. Huang, J. Kosel, Y. Lu and X. X. Zhang, *ACS Appl. Mater. Interfaces*, 2019, **11**, 47091–47097.
32 Y. Shirahata, R. Shiina, D. L. González, K. J. A. Franke, E. Wada, M. Itoh, N. A. Pertsev, S. van Dijken and T. Taniyama, *NPG Asia Mater.*, 2015, **7**, e198.
33 S. Zhang, Y. G. Zhao, P. S. Li, J. J. Yang, S. Rizwan, J. X. Zhang, J. Seidel, T. L. Qu, Y. J. Yang, Z. L. Luo, Q. He, T. Zou, Q. P. Chen, J. W. Wang, L. F. Yang, Y. Sun, Y. Z. Wu, X. Xiao, X. F. Jin, J. Huang, C. Gao, X. F. Han and R. Ramesh, *Phys. Rev. Lett.*, 2012, **108**, 137203.
34 T. Wu, A. Bur, P. Zhao, K. P. Mohanchandra, K. Wong, K. L. Wang, C. S. Lynch and G. P. Carman, *Appl. Phys. Lett.*, 2011, **98**, 012504.
35 M. Buzzi, R. V. Chopdekar, J. L. Hockel, A. Bur, T. Wu, N. Pilet, P. Warnicke, G. P. Carman, L. J. Heyderman and F. Nolting, *Phys. Rev. Lett.*, 2013, **111**, 027204.
36 Y. Ba, Y. Liu, P. Li, L. Wu, J. Unguris, D. T. Pierce, D. Yang, C. Feng, Y. Zhang, H. Wu, D. Li, Y. Chang, J. Zhang, X. Han, J. Cai, C. W. Nan and Y. Zhao, *Adv. Funct. Mater.*, 2018, **28**, 1706448.
37 M. Ghidini, F. Ye, N. J. Steinke, R. Mansell, C. H. W. Barnes and N. D. Mathur, *J. Appl. Phys.*, 2021, **129**, 154101.
38 S. W. Fackler, M. J. Donahue, T. Gao, P. N. A. Nero, S.-W. Cheong, J. Cumings and I. Takeuchi, *Appl. Phys. Lett.*, 2014, **105**, 212905.
39 T.-K. Chung, G. P. Carman and K. P. Mohanchandra, *Appl. Phys. Lett.*, 2008, **92**, 112509.
40 Z. Xiao, K. P. Mohanchandra, R. Lo Conte, C. Ty Karaba, J. D. Schneider, A. Chavez, S. Tiwari, H. Sohn, M. E. Nowakowski, A. Scholl, S. H. Tolbert, J. Bokor, G. P. Carman and R. N. Candler, *AIP Adv.*, 2018, **8**, 055907.
41 M. A. Marioni, N. Pilet, T. V. Ashworth, R. C. O'Handley and H. J. Hug, *Phys. Rev. Lett.*, 2006, **97**, 027201.
42 M. T. Johnsondag, P. J. H. Bloemenddag, F. J. A. den Broederdag and J. J. de Vries, *Rep. Prog. Phys.*, 1996, **59**, 1409–1458.
43 A. Chen, Y. Wen, B. Fang, Y. Zhao, Q. Zhang, Y. Chang, P. Li, H. Wu, H. Huang, Y. Lu, Z. Zeng, J. Cai, X. Han, T. Wu, X. X. Zhang and Y. Zhao, *Nat. Commun.*, 2019, **10**, 243.
44 A. Chen, Y. Zhao, Y. Wen, L. Pan, P. Li and X. X. Zhang, *Sci. Adv.*, 2019, **5**, eaay5141.
45 F. Wang, L. Luo, D. Zhou, X. Zhao and H. Luo, *Appl. Phys. Lett.*, 2007, **90**, 212903.
46 P. Li, A. Chen, D. Li, Y. Zhao, S. Zhang, L. Yang, Y. Liu, M. Zhu, H. Zhang and X. Han, *Adv. Mater.*, 2014, **26**, 4320–4325.
47 A. Chen, Y. Zhao, P. Li, X. Zhang, R. Peng, H. Huang, L. Zou, X. Zheng, S. Zhang, P. Miao, Y. Lu, J. Cai and C. W. Nan, *Adv. Mater.*, 2016, **28**, 363–369.
48 A. Vansteenkiste, J. Leliaert, M. Dvornik, M. Helsen, F. Garcia-Sanchez and B. Van Waeyenberge, *AIP Adv.*, 2014, **4**, 107133.
49 R. Lo Conte, Z. Xiao, C. Chen, C. V. Stan, J. Gorchon, A. El-Ghazaly, M. E. Nowakowski, H. Sohn, A. Pattabi, A. Scholl, N. Tamura, A. Sepulveda, G. P. Carman, R. N. Candler and J. Bokor, *Nano Lett.*, 2018, **18**, 1952–1961.
50 S. Zhang, Y. Zhao, X. Xiao, Y. Wu, S. Rizwan, L. Yang, P. Li, J. Wang, M. Zhu, H. Zhang, X. Jin and X. Han, *Sci. Rep.*, 2014, **4**, 3727.
51 O. Kazakova, R. Puttock, C. Barton, H. Corte-León, M. Jaafar, V. Neu and A. Asenjo, *J. Appl. Phys.*, 2019, **125**, 060901.

52 I. Fina, A. Quintana, J. Padilla-Pantoja, X. Marti, F. Macia, F. Sanchez, M. Foerster, L. Aballe, J. Fontcuberta and J. Sort, *ACS Appl. Mater. Interfaces*, 2017, **9**, 15577–15582.
53 I. Fina, A. Quintana, X. Marti, F. Sanchez, M. Foerster, L. Aballe, J. Sort and J. Fontcuberta, *Appl. Phys. Lett.*, 2018, **113**, 152901.
54 J. D. Clarkson, I. Fina, Z. Q. Liu, Y. Lee, J. Kim, C. Frontera, K. Cordero, S. Wisotzki, F. Sanchez, J. Sort, S. L. Hsu, C. Ko, L. Aballe, M. Foerster, J. Wu, H. M. Christen, J. T. Heron, D. G. Schlom, S. Salahuddin, N. Kioussis, J. Fontcuberta, X. Marti and R. Ramesh, *Sci. Rep.*, 2017, **7**, 15460.
55 D. Nečas and P. Klapetek, *Cent. Eur. J. Phys.*, 2012, **10**, 181–188.